Master's Thesis of Landscape Architecture

The Estimation of Anthropogenic Heat Flux in Seoul, South Korea by remote sensing

원격 탐사를 통한 서울의 인공열 추정

August 2022

Graduate School of Agriculture and Life Sciences

Seoul National University

Landscape Architecture major

Sang Hyuck Kim

The Estimation of Anthropogenic Heat Flux in Seoul, South Korea by remote sensing

Under the Direction of Adviser, Prof. Dong Kun Lee

Submitting a master's thesis of Public Administration

July 2022

Graduate School of Agriculture and Life Sciences
Seoul National University
Landscape Architecture major
Sang Hyuck Kim

Confirming the master's thesis written by
Sang Hyuck Kim
July 2022

Chair Jun seok, Kang (Seal)

Vice Chair Dong kun, Lee (Seal)

Examiner Hee yeun, Yoon (Seal)

Abstract

As urbanization progressed, the amount of heat released to the urban areas are increased. The anthropogenic heat flux (AHF), the heat released by human beings like traffic and energy consumption, become more important to understand the thermal environments of urban areas because of its amount and increasing trends. However there are no accurate method to estimate the AHF in urban areas. By using remote sensing data, we suggest the estimation method that can take the actual thermal conditions of study area. The results show that industrial area have the highest average value of AHF and it is about 130 W/m^2. On the other hand green shows the lowest value, about 10 W/m^2 in average. Between 2019 and 2020, there are a noticeable changes in Gasan digital complex and residential area of Gwanak-gu. The AHF released from the Gasan digital complex was decreased the most in the study area and the AHF released from the residential area of Gwanak-gu was increased the most. During this period, the COVID-19 outbreak began and the government implemented a social distancing policy. Because of this policy, the human activities has been changed and our method can take this situation into consideration very well. Compared with the AHF estimated by energy consumption data, our results show very small difference that 0.13 and 0.22 W/m^2 in average. It confirms that our method has reliable accuracy.

keywords : Anthropogenic heat, Urban heat island, remote sensing, Energy consumption
Student Number : 2020-27283

Table of Contents

Chapter 1. Introduction ····· 1
1.1 Backgrounds and Study purpose ····· 1

Chapter 2. Study Flow and Study Area ····· 3
2.1 Study Flow ····· 3
2.2 Study Area and Input data ····· 5
2.2.1 Study Area ····· 5
2.2.2 Input data ····· 6

Chapter 3. Methods ····· 8
3.1 The energy balance equation ····· 8
3.2 The net radiation estimation ····· 10
3.3 The sensible heat flux estimation ····· 13
3.4 The storage heat flux estimation ····· 15
3.5 The latent heat flux estimation ····· 16
3.6 Validation of AHF estimation methods ····· 18

Chapter 4. Results and Discussion ····· 19
4.1 The AHF estimation in urban areas ····· 19
4.2 The validation of estimation methods ····· 22
4.3 The spatial and temporal changes of AHF ···· 28

Chapter 5. Conclusion ····· 29

Reference ····· 32

Tables

Table 1 Meteorological data used in this study ····· 6
Table 2 The roughness lengths for momentum and heat transport ····· 15
Table 3 The coefficients of various surface types ····· 16
Table 4 The empirical coefficients of surface types ····· 17
Table 5 γ/s values on 1 atm ····· 18
Table 7 The average AHF and standard deviations for each surface types on June 13, 2019 ····· 22
Table 8 The average AHF and standard deviations for each surface types on May 30, 2020 ····· 22
Table 9 The average and standard deviation of the difference between energy consumption and estimated AHF on June 13, 2019 ····· 27
Table 10 The average and standard deviation of the difference between energy consumption and estimated AHF on May 30, 2020 ····· 27

Figures

Figure 1 Study flow chart ····· 4
Figure 2 The location of study area ····· 5
Figure 3 The shadow ratio distribution of Seoul, Korea ····· 7
Figure 4 The surface temperature distribution of Seoul, Korea on June 13, 2019 1100 KST ····· 7
Figure 5 The estimated AHF distribution of Seoul, Korea on June 13, 2019 1100 KST (Unit : W/m2) ····· 19
Figure 6 The estimated AHF distribution of Seoul, Korea on May 30, 2020 1100 KST (Unit : W/m2) ····· 21
Figure 7 The energy consumption distribution of Seoul, on June 2019 (Unit : W/m2) ····· 25
Figure 8 The difference between scaled down energy consumption data and estimated AHF on June 13, 2019 ····· 26
Figure 9 The difference between scaled down energy consumption data and estimated AHF on May 30, 2020 ····· 27
Figure 10 The difference between two estimated results (June 13, 2019 - May 30, 2020) ····· 28

Chapter 1. Introduction

1.1 Backgrounds and study purpose

As urbanization progressed, the proportion of impervious surfaces in urban areas is increasing and it makes cities absorb more heat. As a result, urban areas show higher temperatures than rural areas which is called Urban Heat Island (UHI) and has become the most representative weather in the city (Oke, 1982; Bornstein&Lin, 2000). Along with the UHI, the climate change makes more heat is accumulated in the city, it makes more heat-related diseases and mortalities.

The important variables that affects the UHI include meteorological variables such as temperature, humidity, wind speed, cloude volume and the physical variables such as the size of city, surface roughness length, sky view factor and albedo (Oke 1973; Bornstein 1975; Park et al., 2018; Kwon et al., 2019). Most of studies have been only focused on theses two variables for reducing the UHI. But recently, many studies show that the anthropogenic heat flux (AHF) released from energy consumption by human activities is one of the most important variable of climate changes and UHI (Eaton 1919; Varquez et al., 2021).

Human beings consume various forms of energy in life and production, industy and metabolism (Sailor et al., 2015). The heat released into atmosphere by this energy consumption is called AHF and it makes the near-surface air temperature increased by 1 - 3 ℃ (Gutierrez et al., 2015). The amount of AHF varies from season to country, in some cases, the amount can exceed the radiant heat from

the sun (Kikegawa et al.. 2003; Hamilton et al., 2009). The AHF will not only affect the urban ecological environment but also have an adverse effect on human health and economic development (Chen et al., 2016; Doan et al., 2019; Yuan et al., 2020).

The scale and importance of AHF are increasingly being emphasized, in most study, AHF is assumed '0' because it is too hard to estimate accurately. The urban environment is not only too complex to measure heat flux, but also AHF is commonly measured with heat fluxes like sensible heat flux, so measurements can not accurately determine the amount of AHF (Gabey et al., 2019). Instead of measurement, many studies use the empirical models for estimating AHF in urban areas Sailor and Lu,2004; Smith et al., 2009; Allen et al., 2011; Iamarino et al., 2012; Varquez et al., 2021).

AHF can be estimated either through a top-down approach or a bottom-up approach. For the top-down approach, energy comsumption is coming from a regional or country-level and then scaled down into grided information. The extra data such as population can be needed for down-scale the energy consumption data on high spatial resolutions(Sailor and Lu 2004; Allen et al., 2011). The top-down approach is appropriate when data is insufficient or the study area is large, but the accuracy could be lower because of the data's poor resolution. To handle this problem, most of models try to improve their performance by combined the results from the climate models such as Weather Research and Forecasting Model (WRF) (Flanner, 2009).

Bottom-up approaches estimate the amount of heat emitted from individual buildings and roads, and then expands it to the large scaled study area (Bueno et al., 2012).

This can be show higher accuracy than the top-down approachs,

but it is difficult to estimate accurately because they need the measurement data at various locations (Varquez et al., 2021). Also, as mentioned above, the AHF is difficult to determine the exact amount by measurement, so the top-down approaches is currently mainly used.

Various models are still being developed, but the top-down approaches has a poor spatial resolution of 500 m to 1 km because of the limitation of input data such as energy consumption and populations (Gabey et al., 2019; Varquez et al., 2021; Yu et al., 2021). For this reason, it is difficult to understand the micro scaled thermal environment inside the city, and there is a limit to understanding the exact effects of the AHF and the way how to reduce it. Even if we can get high resolution energy consumption data, the top-down approaches still have errors because of their assumptions. Generally they assume that every equipment have same energy efficiency and the heat generated by energy use are released equally in all directions. However, in real world, the energy efficiencies are different and the heat released from specific points like outdoor unit of an air-conditioner. For better understanding about the thermal environments of urban cities, we need a new estimation method that can take the actual data about the amount and direction of AHF into consideration.

In this study, we suggest the AHF estimation method without any energy consumption or population data. For the estimation, we used surface temperature data from the satellite images to reflect the actual thermal conditions of urban areas. By using Landsat 8 images and land use map, we can estimate AHF with 30 m spatial resolutions and it needs less computational power because of no down-scaling process. Also, it can show more accuracy by taking the

actual data about the amount and direction of AHF into consideration. We verify this method by the average of water and green space's AHF values which expected '0', and compare with energy consumption data.

Chapter 2. Study Flow and Used Data

2.1 Study Flow

This study has three steps (Fig 1). First, we set the study site and collect input data for estimation. Usually, temperature, humidity, wind speed, surface temperature, albedo and digital surface model (DSM) are needed to estimate AHF in urban areas. The surface temperature and albedo can be acquired by satellite images and using Korea Meteorological Administration's (KMA) data for other meteorological data like temperature. Second, we estimate AHF in study sites by suggested method. Finally, we validate our results by comparing with energy consumption data.

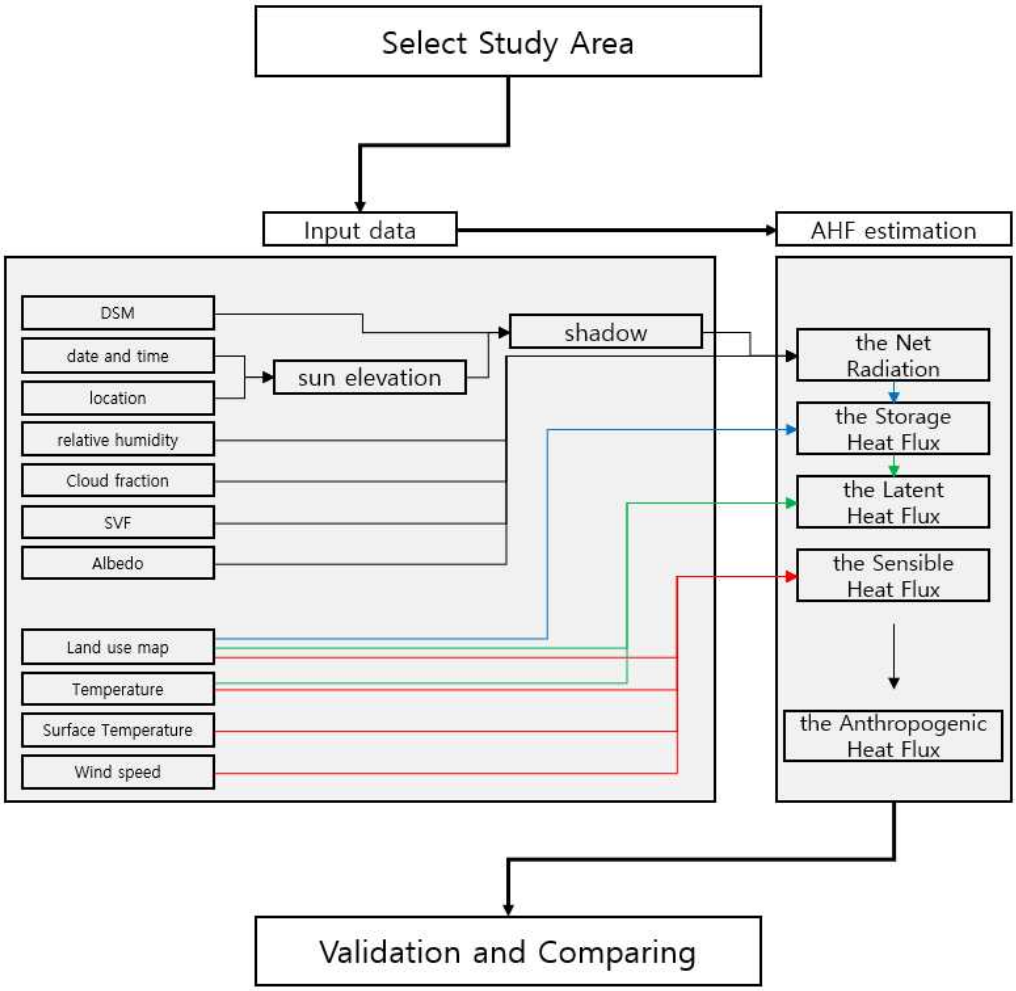

Figure 1 Study flow chart

2.2 Study areas and input data

2.2.1 study area

The city of Seoul, South Korea, an area of approximately 605 km2 was chosen as a study area to estimate the AHF. Seoul is the city with the highest population density and about 20% of the total population of South Korea. There are a total of 4 million households,

3.1 million vehicles are registered and energy use is second among Korean cities, following Ulsan, the largest industrial city in South Korea. Seoul is expected to release the most AHF inside the city due to the large number of buildings and traffic, and three industrial complexes are located which is expected to allow comparison between residential areas and industrial complexes.

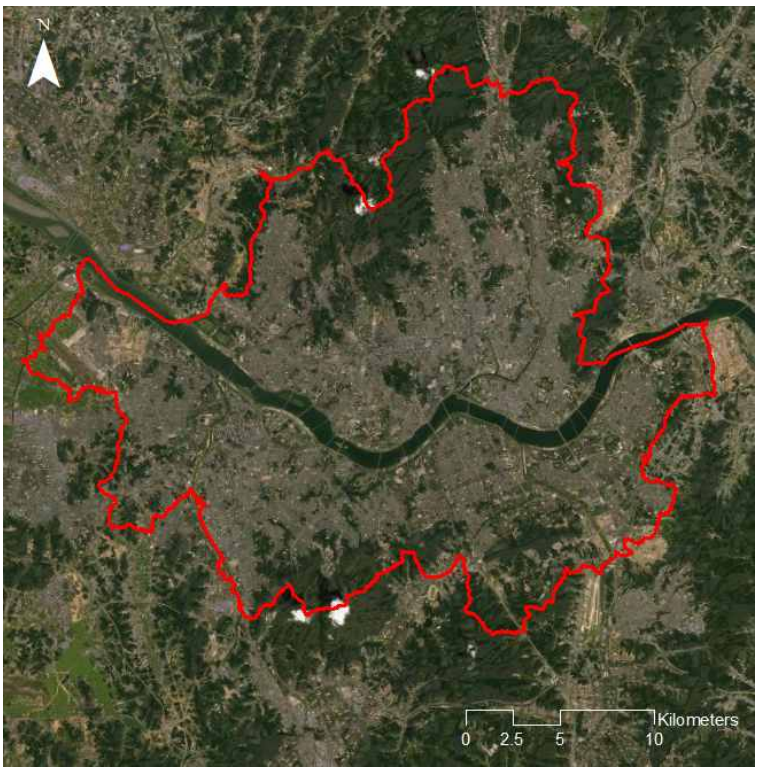

Figure 2 The location of study area

2.2.2 Input data

Automatic Weather Station(AWS) data which were provided by KMA are used for estimating various heat fluxes such as sensible heat flux, latent heat flux and storage heat flux. The meteorological data like temperature and wind speed are provided in point data, we

interpolated this data by IDW (Inverse Distance Weighted) method for making 30 m raster data of Seoul.

Input data	Parameter	Units
Air temperature	T_a	℃
Wind speed	u_a	m/s
Relative humidity	RH	%
Air pressure	P_{atm}	Pa

Table 1 Meteorological data used in this study

The shadow ratio which is used for calculating solar and net radiation were calculated by Hillshade tools in Arcgis 10.5. Actual shadow areas of buildings and other urban contexts were calculated by 1 m spatial resolution, and then average by 30 m grid for same spatial resolution with Landsat 8 images. The DSM used for Hillshade tools were made by digital map by National Geographic Information Service of Korea.

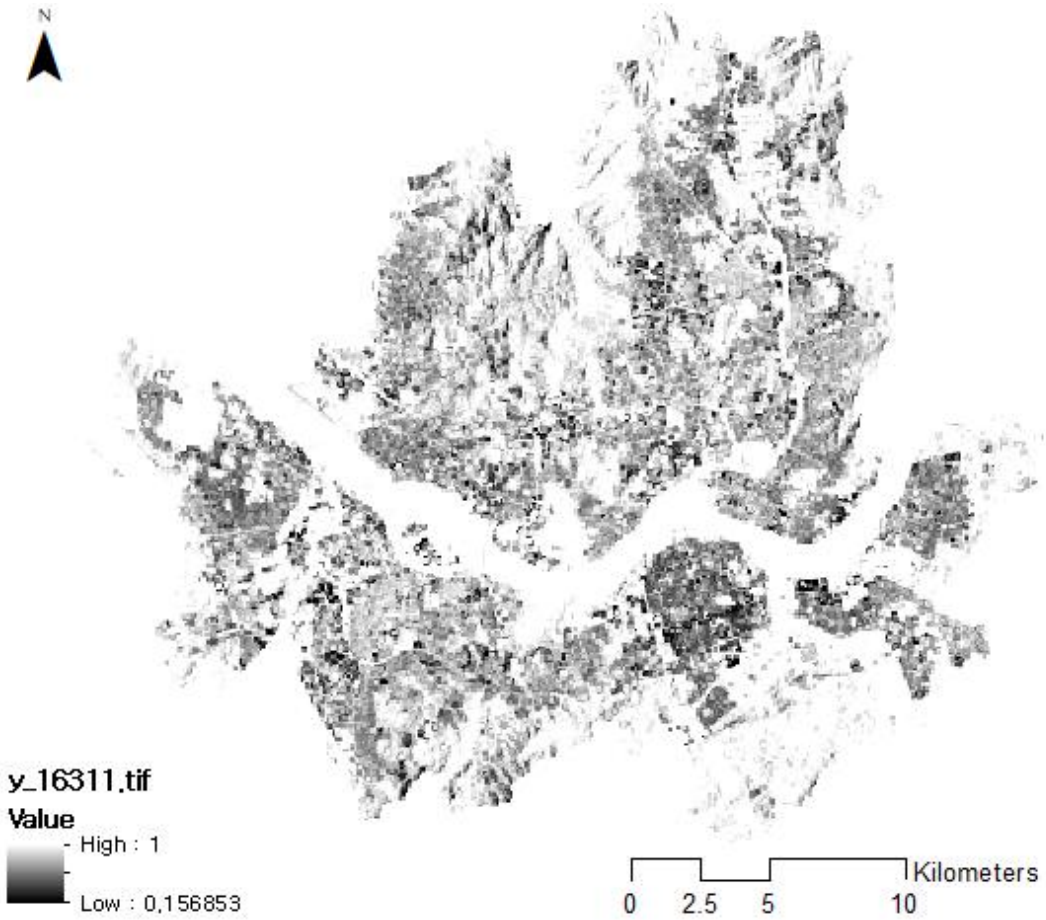

Figure 3 The shadow ratio distribution of Seoul, Korea

The Landsat 8 OLI/TIRS (Operational Land Imager/Thermal Infreared Sensor) images were used for surface temperature and albedo. Landsat 8 Collection 2 level 2 Science Product (L2SP) data by United States Geological Survey (USGS) were used in this study which have been pre-processed. We use Landsat images in summer seasons (June to August) which were expected to have the highest AHF, with less than 5% cloud fractions.

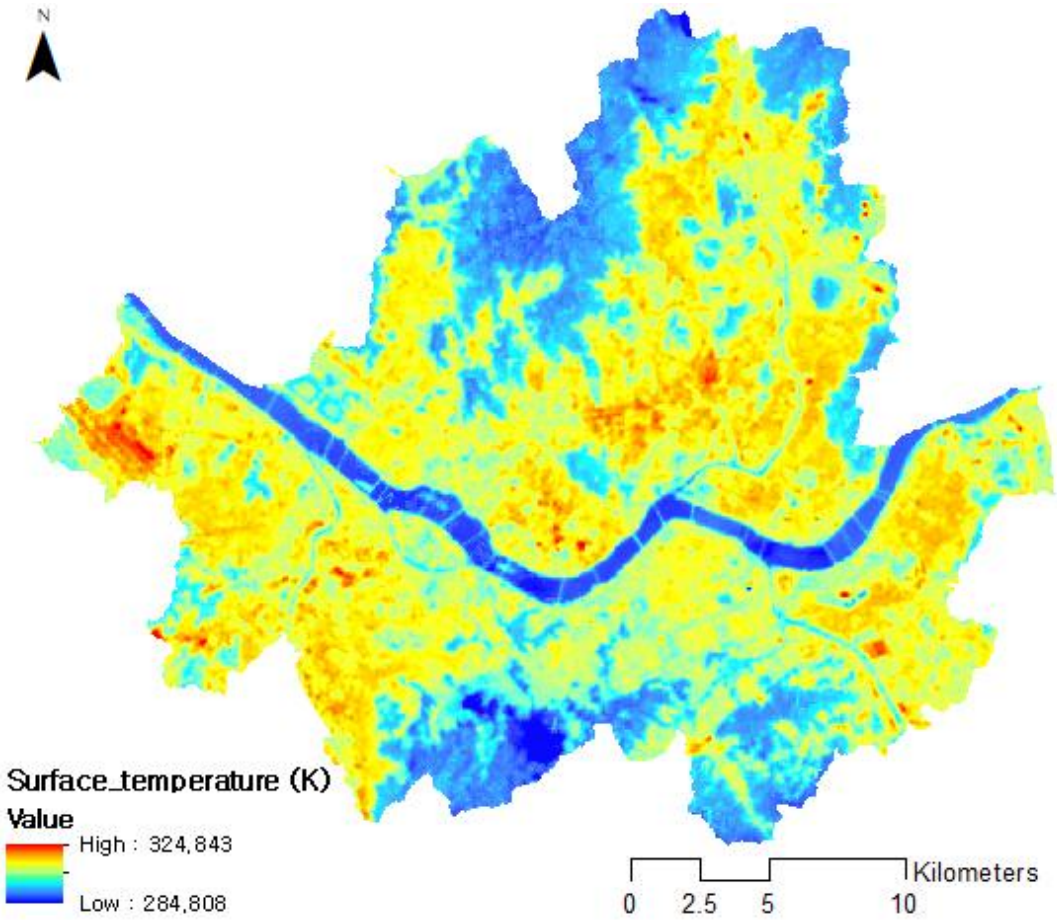

Figure 4 The surface temperature distribution of Seoul, Korea on June 13, 2019 1100 KST

Chapter 3. Methods

3.1 The energy balance equation

The radiations which was reached to the urban surfaces are absorbed or emitted by various forms, and it should follow the energy balanced equation. (eq 1)

$$Q_n + A = H + \lambda E + Q_s \qquad \text{Equation 2}$$

where Q_n means net radiation, A means AHF, H means sensible heat flux, λE means latent heat flux, Q_s mean storage heat flux. The equation means that short or long-wave radiations reached to the urban surfaces are absorbed or emitted to atmosphere by sensible, latent or storage heat flux.

Most of the short-wave radiations in urban areas are solar radiations. The short-wave radiation has a greater energy than long-wave radiation, making up most of the urban area's heat (Kato et al., 2005). The long-wave radiations are emitted by all objects which have surface temperature. There are a lot of sources which emits the long-wave radiation, but it has less energy than the short-wave radiation.

The AHF is mainly released by the form of long-wave radiation to atmosphere. It does not directly emitted to urban surfaces, was absorbed by atmosphere(Gutierrez et al., 2015). So AHF increases the air temperature and make the atmosphere emits more long-wave radiations.

The AHF mainly released to the area that was consist of impervious surfaces. The impervious surfaces in urban contexts have a tiny amount of waters so there are little increases of the latent heat fluxes with extra incoming radiations (Kato et al., 2005). The storage heat fluxes can be increased by extra incoming radiations, but the long-wave radiation increased by AHF is much smaller than the solar radiations, so there is no problem that assumed the increased storage heat flux is '0' by AHF (Kato et al., 2005; Wong et al., 2015). In other words, all of the AHF released to urban areas become sensible heat fluxes (Kato et al., 2005).

Therefore, when we estimates the AHF by energy balance

equations, the latent heat flux and storage heat flux do not need to consider the effect of AHF. However, the sensible heat fluxes have to include AHF effects when estimated. Then, we can estimate the AHF by equation 2:

$$A = H + LE + Q_s - Q_n$$ Equation 2

3.2 The net radiation estimation

The net radiation mostly affected by the solar elevation which is determined by the date, time and locations. By these variables, the Extraterrestrial radiation for hourly periods can be calculated (Allen et al., 1998):

$$R_a = \frac{12 \times 60}{\pi} G_{sc} d_r [(\omega_2 - \omega_1)\sin(\varphi)\sin(\delta) + \cos(\varphi)\cos(\delta)(\sin(\omega_2) - \sin(\omega_1))]$$

Equation 3

where R_a means extraterrestrial radiation (MJ m^{-2} $hour^{-1}$), G_{sc} is solar constant (= 0.082 MJ m^{-2} min^{-1}), δ is solar declination (rad), φ is latitude (rad), d_r indicates inverse relative distance Earth-Sun that are given by (Allen et al., 1998):

$$\delta = 0.409 \sin(\frac{2\pi}{365} J - 1.39)$$ Equation 4

$$d_r = 1 + 0.033 \cos(\frac{2\pi}{365} J)$$ Equation 5

where J is Julian date, ω_1 and ω_2 are given by(Allen et al., 1998):

$$\omega = \frac{\pi}{12}[(t + 0.06667(L_z - L_m) + S_c) - 12]$$
$$\omega_1 = \omega - \frac{\pi t_1}{24}$$
$$\omega_2 = \omega + \frac{\pi t_1}{24} \qquad \text{Equation 6}$$

where t is standard clock time at the midpoint of the period (hour), L_z is longitude of the centre of the local time zone (degrees west of Greenwich), L_m is longitude of the measurement site (degrees west of Greenwich), S_c is seasonal correction for solar time (hour)

The clear-sky solar radiation can be calculated by (Allen et al., 1998):

$$R_{so} = (0.75 + 2*10^{-5}z)R_a \qquad \text{Equation 7}$$

where z is elevation above sea level.

To estimate the net radiation of urban surfaces, the direct short-wave radiation and the diffuse short-wave radiation should be calculated by the clear-sky solar radiation. The direct short-wave radiations are affected by shadows and the diffuse short-wave radiations are affected by Sky View Factor (SVF). S_{dir} and S_{diff} are given by (Allen et al., 1998):

$$S_{diff} = R_{so}*(0.3 + c(F_{CLD})^d)$$
$$S_{dir} = R_{so} - S_{diff} \qquad \text{Equation 8}$$

where F_{CLD} is cloud fraction that is given by (Loridan et al., 2011):

$$F_{CLD} = 0.185[e^{(0.015 + 1.9 \times 10^{-4} \times T_a) \times RH} - 1] \qquad \text{Equation 9}$$

where RH is relative humidity, T_a is air temperatrue. Now we can calculate the net short-wave radiation of urban surface by:

$$S_{net} = (Shadow * S_{dir} + SVF * S_{diff}) * (1 - \alpha) \qquad \text{Equation 10}$$

where $Shadow$ is the shadow ratio, SVF is sky veiw factor, α mean albedo.

In this study, we focused on the heat fluxes between urban surfaces and atmosphere, so we assumed all of the urban contexts' surface as one layer. In the other words, the atmosphere is only one incoming long-wave radiations source to urban surfaces, and it is calculated by (Offerle et al., 2003; Loridan et al., 2011):

$$L\downarrow = [\varepsilon_{clear} + (1 - \varepsilon_{clear}) \times F_{CLD}] \times \sigma T_a^4 \qquad \text{Equation 11}$$

where $L\downarrow$ is incoming long-wave radiation, ε_{clear} is the emissivity of clear-sky. The long-wave radiation that objects are emitted is determined by the object's surface temperature. The actual air temperature has changed by the elevation, but it is too complicated to estimate and it is beyond this study's extent. So we assumed the atmosphere to single layer, calculate emitted long-wave radiation by air temperature (Loridan et al., 2011). For more accurate estimation, the air temperature and the effects of clouds should be considered. The emissivity of clear-sky can be changed by the air temperature and it is given by:

$$w = 46.5(e_a / T_a)$$
$$\varepsilon_{clear} = 1 - (1 + w)e^{-\sqrt{1.2 + 3w}} \qquad \text{Equation 12}$$

where w is perceptible water, e_a is vapor pressure. The emitted long-wave radiation from the urban surfaces can be calculated by Stefan-Boltzmann law:

$$L\uparrow = \varepsilon_s \sigma T_s^4 + (1 - \varepsilon_s)L\downarrow \qquad \text{Equation 13}$$

where Lup is the emitted long-wave radiation from the urban surfaces, Ts is surface temperature, e is the emissivity of surface. The net long-wave radiation of urban surfaces can be calculated by subtraction between incoming long-wave radiation and emitted long-wave radiation from the urban surfaces.

$$L_{net} = L\downarrow - L\uparrow \qquad \text{Equation 14}$$

Also, the net radiation is given by:

$$R_n = S_{net} + L_{net} \qquad \text{Equation 15}$$

3.3 The sensible heat flux estimation

The sensible heat was used to change a temperature of material, its flux between two objects can be calculated by physical properties like temperature, specific heat and density. Especially, the sensible heat fluxes between urban surfaces and atmosphere can be estimated by equation 3:

$$H = \rho C_p \frac{T_s - T_a}{r_a}$$ Equation 16

where ρ indicates air density, C_p indicates specific heat of air, T_a means air temperature, T_s means surface temperature of the urban surfaces. As mentioned before, the surface temperature of the urban surfaces were acquired by Landsat 8 images which can be said that contains the AHF effects, so it is appropriate to estimate the sensible heat flux. r_a is the aerodynamic resistance which is calculated by wind speed, land cover, obstacles height (Brutsaert, 1982).

$$r_a = \frac{\ln(z_u - d_0) - \psi_M}{z_{0M}} * \frac{\ln(z_u - d_0) - \psi_H}{z_{0H}} * \frac{1}{k^2 u}$$ Equation 17

where z_u is the height of temperature and wind speed are measured, u is wind speed, k is von Karman's constant (= 0.4), z_{0M} and z_{0H} are the roughness lengths for momentum and heat transport, respectively. All measurements are in meters. d_0 means zero-plane displacement that is calculated using the method proposed by Macdonald et al. (1988):

$$d_0 = z_h\{1.0 + A^{-\lambda P}(\lambda P - 1.0)\}$$ Equation 18

where z_h means the height of obstacles, A is the constant (= 4.43 for staggerd arrays), λP is the plan area density of obstacles. The roughness lengths for momentum and heat transport used are listed in Table 2.

Land cover	Z_{0M}	Z_{0M}/Z_{0H}
Water	$0.3 * 10^{-4}$	0.34
Bare soil	0.001	50
Field	0.004	50
Grassland or Rice field	0.1	100
Lawn	0.01	50
Forest	0.5 - 1.0	1000
Suburban	0.5	1000
Urban	1.5	1000
Industrial	0.9	1000

Table 2 The roughness lengths for momentum and heat transport

3.4 The storage heat flux estimation

For the accurate estimation of the storage heat flux, we need all urban surfaces thermal properties such as conductivity and heat capacity. But it is impossible to acquire such data about the whole city because there are too many kinds of surfaces and they are mixed. To handle this difficulties, many studies develop the storage heat flux estimation method by relationship with the net radiation. This study adopted objective hysteresis model (OHM) which is most widely using model to estimate stroage heat flux, proposed by Grimmond et al., (1991a). The model has been captured the hysteresis pattern of the diurnal relation between the net radiation and the storage heat flux, and estimate the storage heat flux by:

$$Q_s = a_1 Q_n + a_2 \Delta Q_n + a_3 \qquad \text{Equation 19}$$

where ΔQ_n is the $(Q_{t+1} - Q_{t-1})/2$, a_1, a_2, a_3 is the coefficients of surface type. In the urban areas, there are a lot of differenct surface

types in one grid, so the storage heat fluxs are given by:

$$Q_s = \sum_{i=1}^{j} f_i * [a_{1i} Q_n + a_{2i} \Delta Q_n + a_{3i}] \qquad \text{Equation 20}$$

where f_i is the fraction of ith surface type. a_{1i}, a_{2i}, a_{3i} is the coefficients ith surface. For 30 m spatial resolution, the fraction of all surface types in 30 m dimension should be calculated first. The coefficients of surfaces used are listed in Table 3.

Land cover	a_1	a_2	a_3
Building	0.12	0.39	−7.17
Road	0.61	0.41	−27.7
Impervious surface	0.7	0.33	−38
Bare soil	0.37	0.42	−34.9
Lawn	0.32	0.54	−27.4
Forest	0.11	0.11	−12.3
Water	0.5	0.21	−39.1

Table 3 The coefficients of various surface types

3.5 The latent heat flux estimation

For estimate the latent heat flux, the vapor pressure deficit, aerodynamic resistance and stomatal resistance should be calculated. However, calculating the stomatal resistance in urban areas is very complicated (Kato & Yamaguchi, 2005). So this study adopted the simple parameterization method proposed by De Bruin & Holtslag (1982) which is based on the Penman-Monteith method. The latent heat flux is given by:

$$\lambda E = \frac{\alpha}{1+(\gamma/s)}(Q_n - S) + \beta \qquad \text{Equation 21}$$

where α, β is the empirical coefficients of surface types and these are listed in Table 4 (Hanna & Chang 1992; Grimmond & Oke, 2002).

Land cover	α	β
Building	0	20
Road	0.2	20
Impervious surface	0.2	20
Bare soil	0.4	20
Lawn	0.8	20
Forest	1.0	20
Wet land	1.2	20
Water	1.3	20

Table 4 The empirical coefficients of surface types

s indicates the slope of the saturation-vapor-pressure temperature curve, γ means the psychrometric constant ($= 0.67 \times 10^3$). At 1 atm, γ/s values are listed in table 5 (Beljaars, 1989; Holstag & Ulden, 1989).

T_a (℃)	γ/s	$\frac{\gamma/s}{1+\gamma/s}$
−5	2.01	0.67
0	1.44	0.59
5	1.06	0.51
10	0.79	0.44
15	0.60	0.38
20	0.45	0.31
25	0.35	0.26
30	0.27	0.21
35	0.21	0.17

Table 5 γ/s values on 1 atm

3.6 Validation of AHF estimation methods

There are two steps for validation the methods. First, estimation about the water and green spaces surface types which are expected to be '0' AHF are evaluated. The average of AHF should be 0 at natural surfaces because there are no sources that can release AHF. Therefore, the average and standard deviation of AHF in water and green spaces can be an indication of the accuracy of estimation. Second, estimated AHF compared with the actual energy consumption data. The monthly energy consumption data by a lot number are provided by the Ministry of Land, Infrastructure and Transport of Korea. By down-scaled this data, we can estimate the AHF very roughly and compared with the estimation results. In this study, we down-scale the monthly energy consumption data based on the profiles proposed by KEMCO (2002). Between energy consumption and AHF released, there are a lag time and all energy consumption

become AHF. However, it is very complicated to specify and is not a main goal of our study, so these are ignored in this study.

Chapter 4. Results and Discussion

4.1 The AHF estimations in urban area

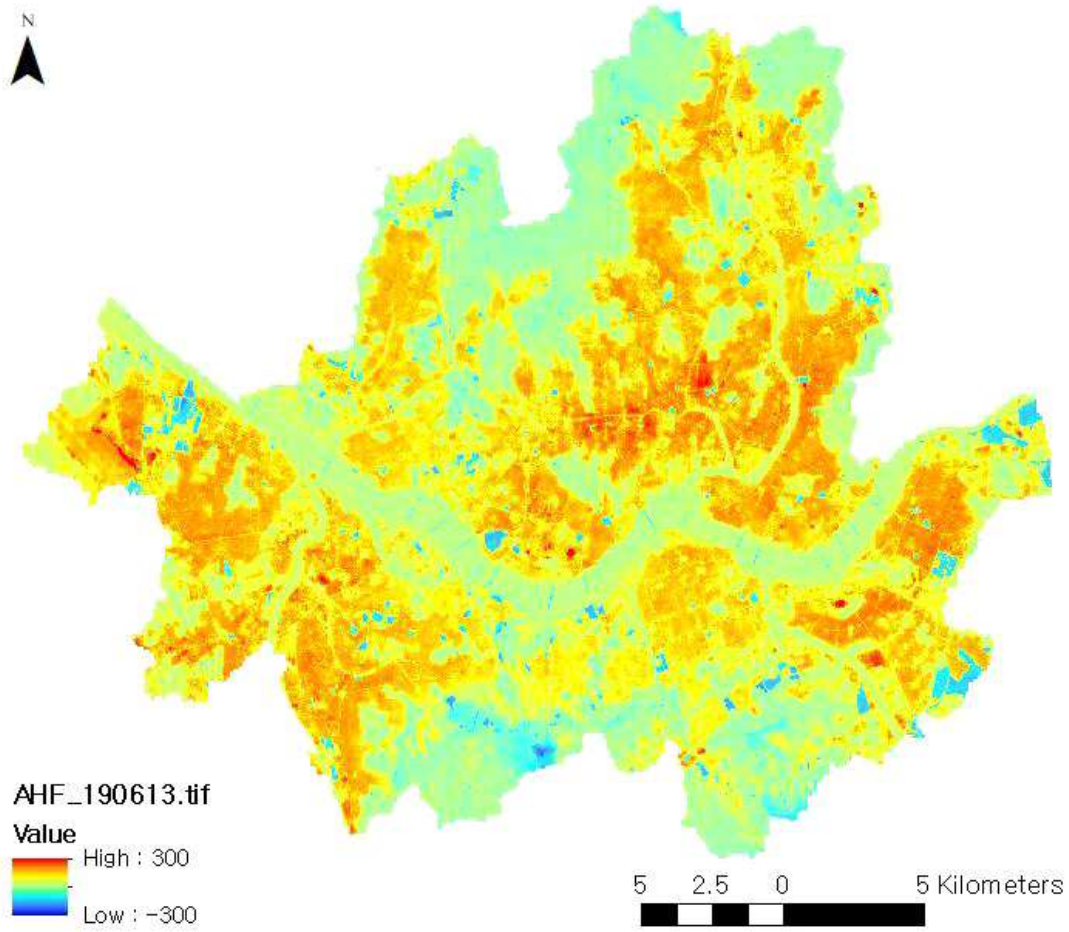

Figure 5 The estimated AHF distribution of Seoul, Korea on June 13, 2019 1100 KST (Unit : W/m^2)

The AHF on June 13, 2019 and May 30, 2020 estimated by the method (Eq 2) are shown in Figs 5 and 6. According to Eq. 2, for estimating the AHF, various heat flux such as the sensible heat flux and the latent heat flux should be estimated before. All three estimation method of heat flux can contain errors in the estimate equation it self, and the input variables also have an errors. For instance, Landsat images have 30 m spatial resolutions and it can be a problem where various type of surfaces are mixed in a complicated way that the all surfaces have the same surface temperature. Also, the land use map's classification could make errors. In this study area, minimum value of AHF are shown in the bottom of the images that is classified as urban areas. Actually, it is a part of mountains so it's surface temperature was low and sensible heat flux was estimated to a very small values. However, the latent heat flux also estimated small because they were classified as urban area. For this reason, the minimum AHF value was estimated in this area that produce error of about -200 W/m^2.

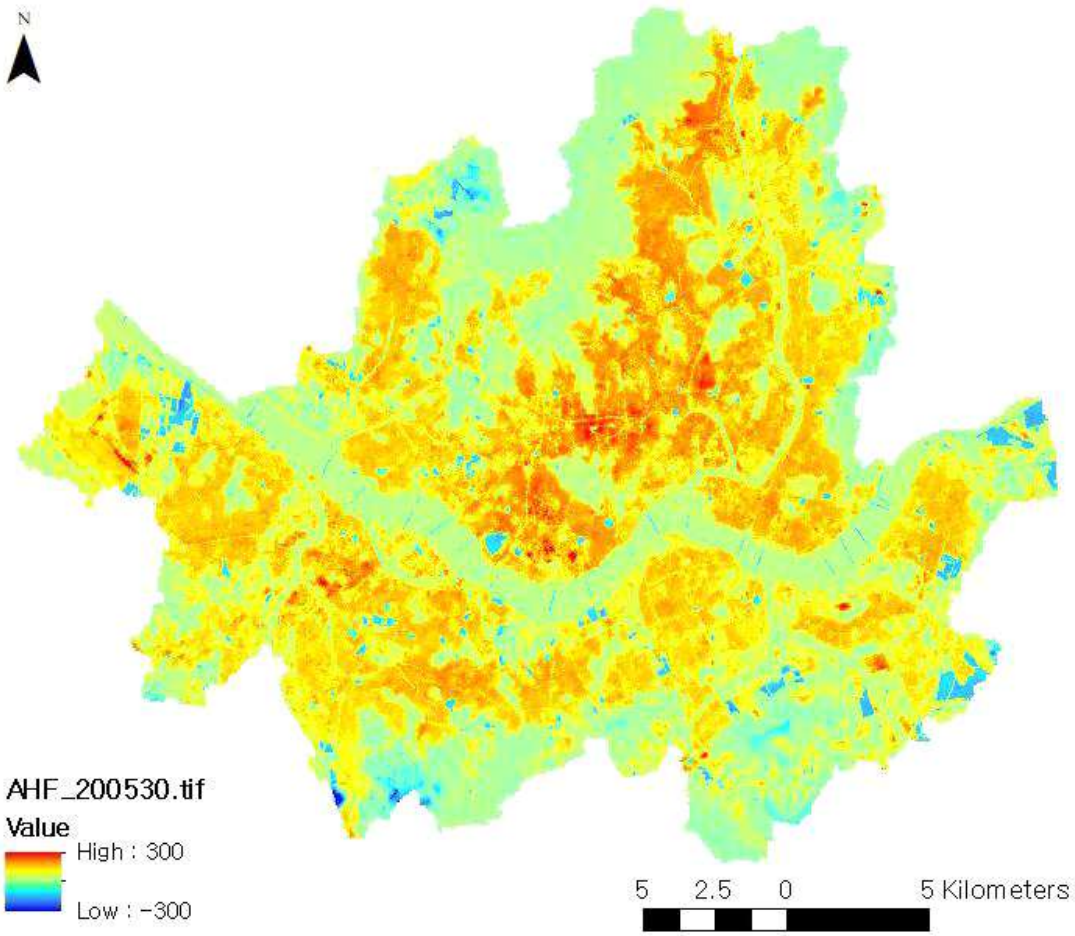

Figure 6 The estimated AHF distribution of Seoul, Korea on May 30, 2020 1100 KST (Unit : W/m^2)

As the estimation results shown in Fig 5 and 6, the area where the most AHF is released was an industrial area which is situated in the south-west part of the study area. There is the Gasan digital complex which is the only national industrial estate in Seoul and it shows the highest AHF in both results. The other areas that show the high AHF values are the areas that various commercial buildings and offices were located with a large floating population such as Gangnam and Jongno. In the residential areas, a low-rise high density areas show higher AHF values than an apartment area.

Above things show the results is quite reasonable and is consistent with the general perception.

4.2 The validation of estimation method

June 13, 2019		
Land cover	Mean	Standard deviation
Urban	125.3	62.8
Road	93.5	67.3
Industrial	135.6	49.3
Bare soil	-57.3	49.6
Green	9.9	36.8
Water	24.7	21.5

Table 8 The average AHF and standard deviations for each surface types on June 13, 2019

May 30, 2020		
Land cover	Mean	Standard deviation
Urban	120.7	62.1
Road	88.2	68.3
Industrial	109.5	47.6
Bare soil	-48.1	66.5
Green	10.8	38.1
Water	19.6	31.1

Table 9 The average AHF and standard deviations for each surface types on May 30, 2020

The average AHF and standard deviations for each surface types are listed in Table 7 and 8. The natural surfaces like bare soil, green and water which have no human activities are expected to have '0' AHF, so the average and standard deviation of natural surfaces can

show the accuracy of the estimation method very roughly.

Following the results, bare soil, green, water surface types show about -50, 10, 20 W/m^2 on the average and their standard deviations are about 60, 35, 25 W/m^2 respectively. This did not fully coverage to zero as theoretically expected due to errors in the data and methods, but this allows us to identify the range of errors that can be made by this estimation method.

In the case of water, the mean value was the second closest to zero in both results and the lowest standard deviation was shown. This is the most ideal result among all surface types, and it was confirmed that the water related estimation method of the latent heat flux and the storage heat flux were quite accurate. It is expected that the slight error occurred when estimating the sensible heat flux, and the cause is that the temperature above water was higher than the actual temperature in the process of interpolating AWS data, so the sensible heat flux could be overestimated.

The green surfaces show little bit lower AHF values than the water. Their average is about 10 W/m^2 and standard deviation is about 35 W/m^2, also they showed good results with the theoretical expectation. However, in areas adjacent to urban surfaces were shown the high AHF values which is presumed to be due to the overestimation of the surface temperature at the boundary because of the resolution of satellite images. Also, most of green surfaces located in the edge of the study site, the standard deviation can be relatively higher in the process of interpolating the AWS data.

The bare soil is the only surfaces that show negative average values. This means that the sum of three estimated heat fluxes were smaller than the calculated net radiation, and it can be thought that it was underestimated in all heat fluxes. Maybe the error was relatively

large because most studies related to the latent heat flux and storage heat flux did not mainly focus on bare soils.

The area which shows the highest AHF on average is the industrial area, showing about 130 W/m^2. It is much higher than the other impervious surfaces in urban areas because of the characteristics of the industrial areas that use more energy than the other spaces.

The other urban areas show the second highest average AHF values, about 120 W/m^2. In the case of road, it is thought that the narrow width resulted in a large error because of the limited resolution of satellite images. The road shows very similar average values to the average of green in both results. This is an error caused by the spatial resolution of satellite, 30 m, that is too large to accurately capture the surface temperature of the road, and it could be underestimated because of the plants such as street trees around the road. Also, this study did not estimate the AHF form the traffics, the estimated AHF of the road should be smaller than actual value.

In all surface types, the results show significantly high standard deviation values. Because of the shadows of buildings, the net radiations are fluctuated in the same surface type. The difference of net radiation can be over 300 W/m^2 by only shadows and it can change the sensible, latent, storage and anthropogenic heat flux over 100 W/m^2. In study area, there are a lot of high rise buildings and their density is also high. Because of this reason, the standard deviation can show high values but we cannot say it was wrong or inaccurate.

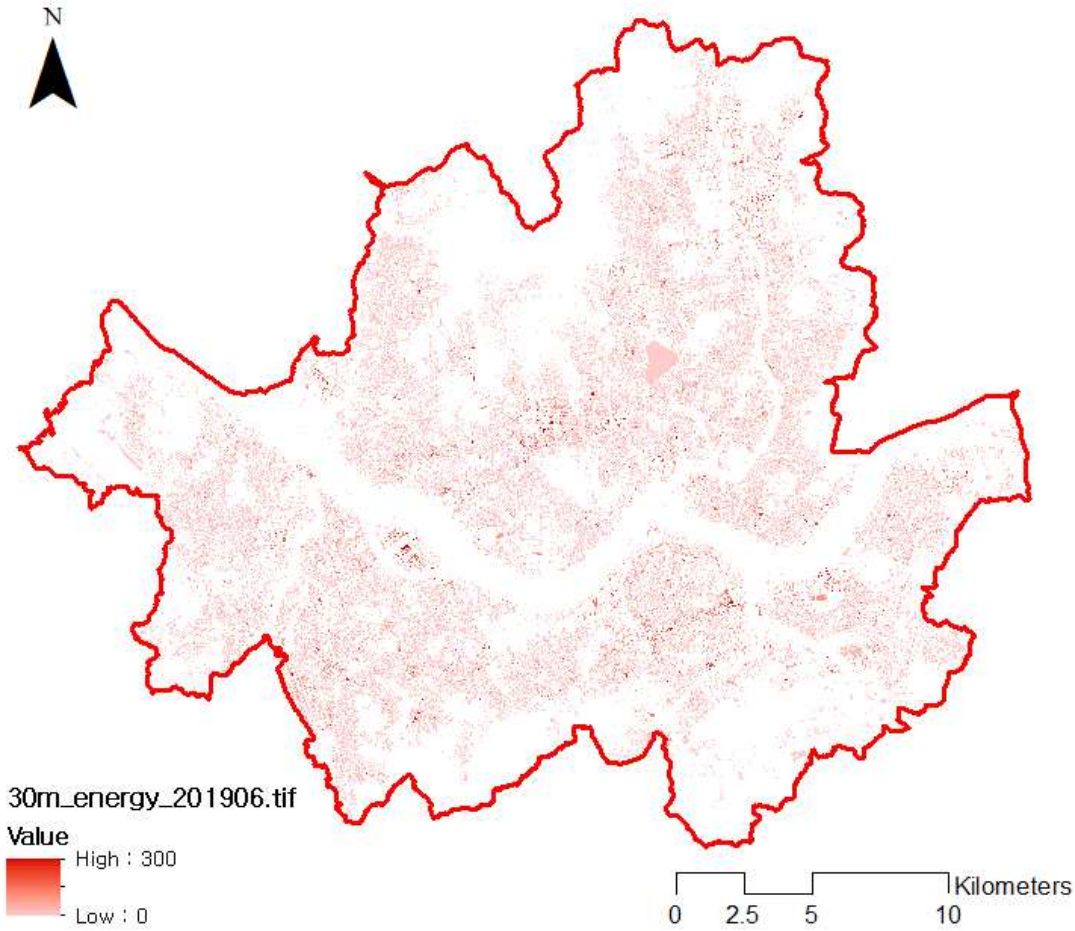

Figure 7 The energy consumption distribution of Seoul, on June 2019 (Unit : W/m^2)

A total of 140,000 energy consumption data were mapped for validating the estimation. For excluding errors from comparison with pixels without energy consumption data, remain 'Nodata' instead of mapping to zero values.

Compare with the estimation results from suggested method, energy consumption data shows very similar distribution on study site. The difference between scaled down energy consumption data and estimated AHF are 0.02 and -0,55 on average. Compare to the average value that very close to zero, the standard deviation was

slightly higher, which is thought to be due to the presence of errors in the energy consumption and building information data. For instance, the maximum difference between two results is 12,085 W/m^2, occuring from the building that recorded 0.08m^2 plan area but using huge amount of energy. That building's actual plan area is about 400 m^2, so if there are more accurate data can constructed or obtained, better validation can be progresssed

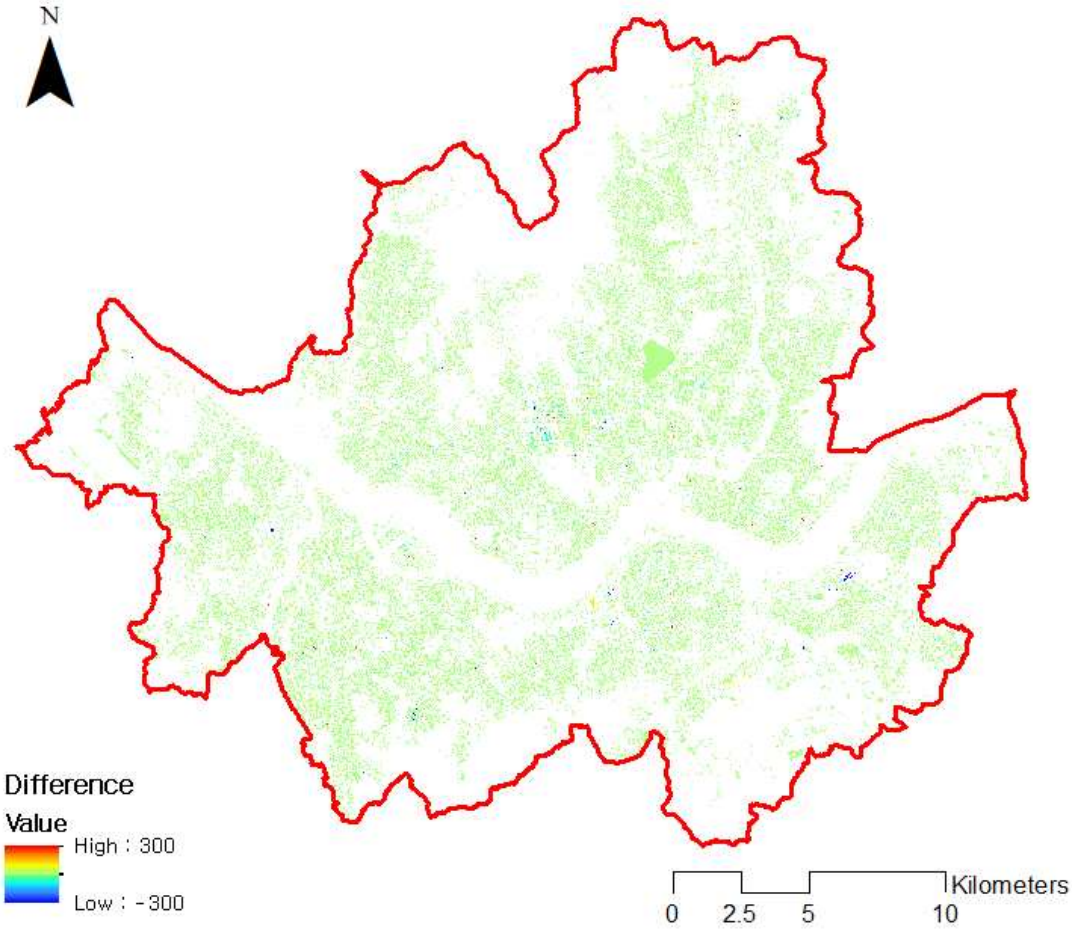

Figure 8 The difference between scaled down energy consumption data and estimated AHF on June 13, 2019

June 13, 2019	
Mean	Standard deviation
0.13	51.1

Table 10 The average and standard deviation of the difference between energy consumption and estimated AHF on June 13, 2019

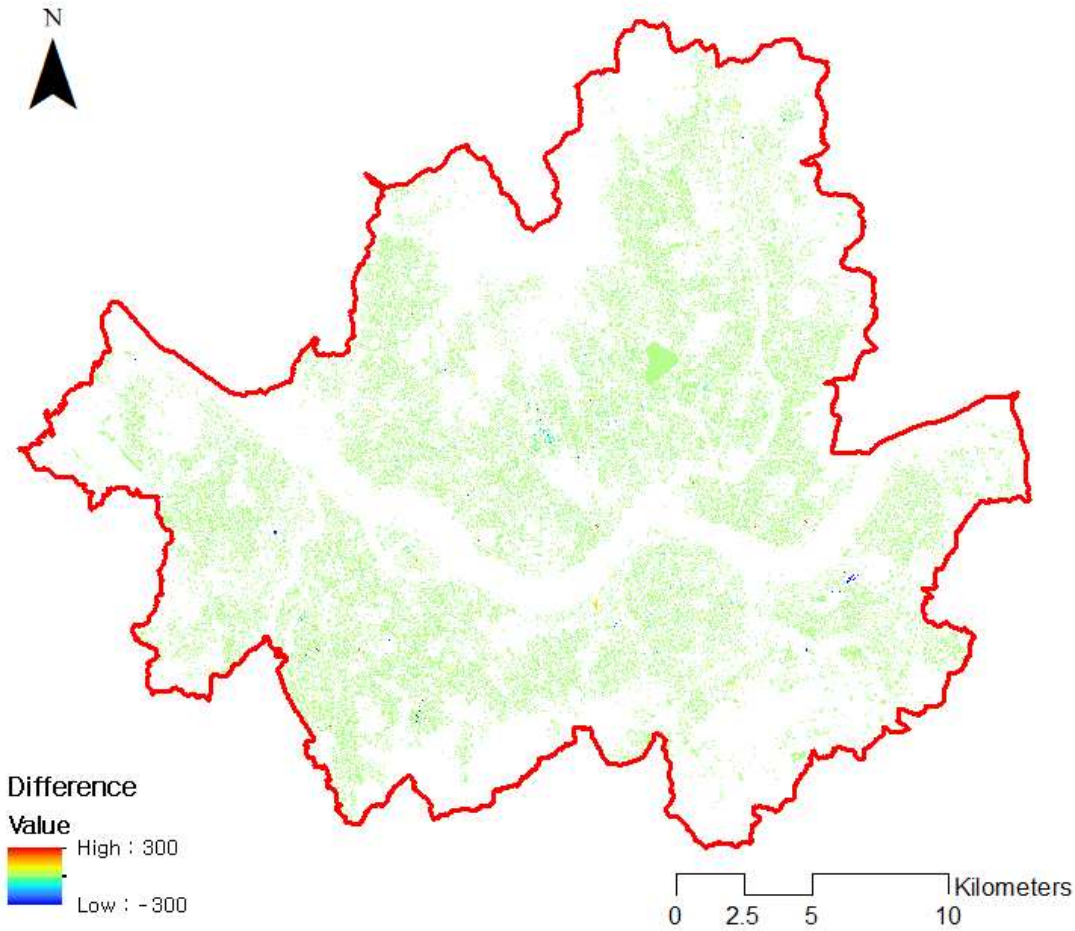

Figure 9 The difference between scaled down energy consumption data and estimated AHF on May 30, 2020

May 30, 2020	
Mean	Standard deviation
0.22	47.3

Table 11 The average and standard deviation of the difference between energy consumption and estimated AHF on May 30, 2020

4.3 The spatial and temporal changes of AHF

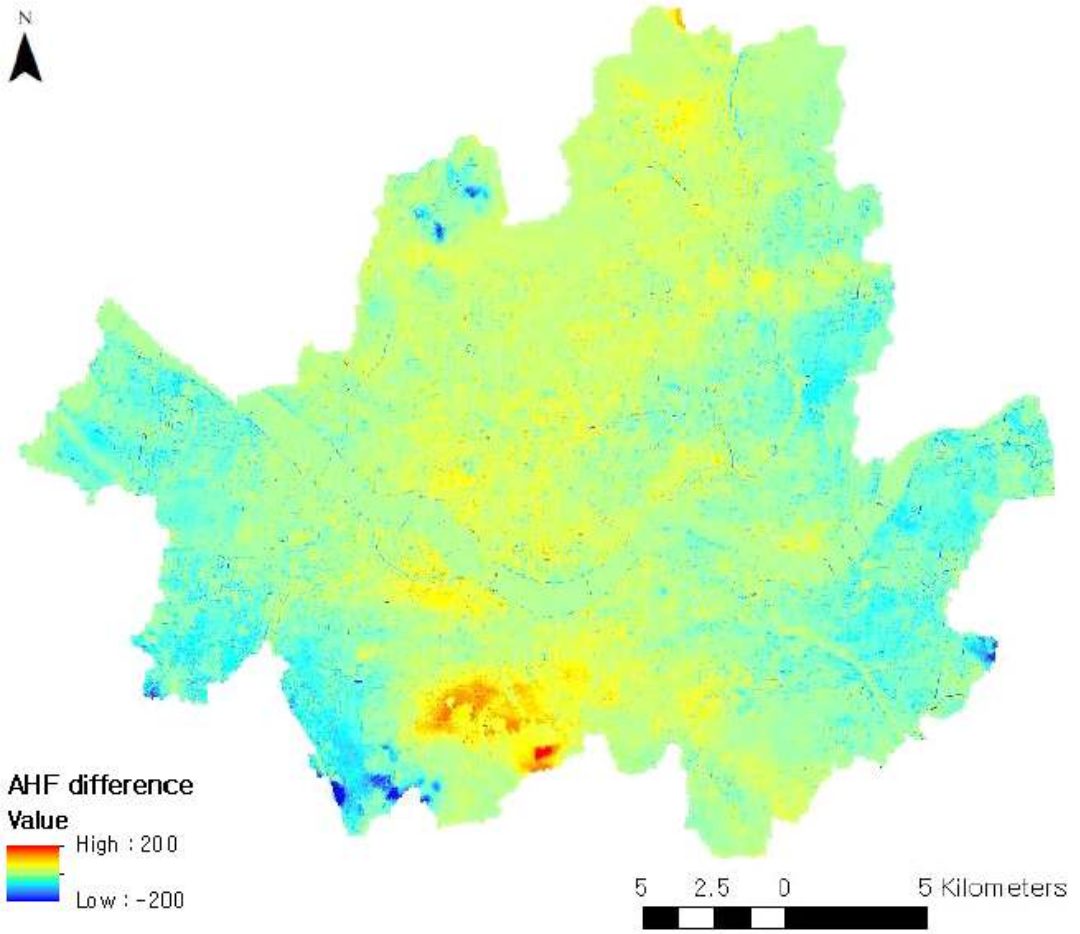

Figure 10 The difference between two estimated results (June 13, 2019 - May 30, 2020)

Between 2019 and 2020, there are a noticeable changes in Gasan

digital complex and residential area of Gwanak-gu. The AHF released from the Gasan digital complex was decreased the most in the study area and the AHF released from the residential area of Gwanak-gu was increased the most. During this period, the COVID-19 outbreak began and the government implemented a social distancing policy. This policy has led to a lot of people working from home and it makes the AHF value on industrial area decreased. Because of this trend, people spend more time at home and it makes the AHF on residential area become increased. In addition to industrial areas, the decrease in AHF was confirmed in downtown areas such as Gangnam and Jongno, and the increase in AHF in residential areas at the top of the study area was confirmed.

Through these results, the COVID-19 had various effects not only on the way of life of the city dwellers, but also the ecosystem of urban areas such as thermal environment.

Chapter 5. Conclusion

From the energy balance equation, the anthropogenic heat flux (AHF) can be estimated by meteorological data, satellite images and land use map. We estimate the AHF on the urban areas and show that our results are quite reasonable. In order to compare and validate the estimation results, we mapped about 140,000 buildings the hourly energy consumption data by down scaled the monthly actual usage.

The estimated AHF distribution of Seoul corresponded reasonably well with the energy consumption data. The difference between two datas are almost 0 on average (actually 0,02 and -0.55 W/m^2), and the standard deviation is about 68 W/m^2. The AHF was highest in the industrial area, and lowest in the water. The estimated AHF in

water was about 20 W/m^2 on average, that is very close to theoretical values, the zero. This implies that our results are quite resonable and it is possible to estimate the AHF by remote sensing. The industrial area show the highest average value of AHF, and it is much larger than the other impervious surfaces in urban areas. In industrial areas, the average AHF is about 130 W/m^2 and it is about 20% of the net radiation in open area that has no shadows. This can make serious problems when we evaluate the thermal environments of urban cities without considering the AHF. Through this results, it could be thought that our method can reflect the amount of energy consumption appropriately.

Between 2019 and 2020, we can found the noticeable changes in the spatial distribution of the AHF. Because of the COVID-19 outbreak and the social distancing policy from the government, a lot of people working from home and it makes people spend more time on residential areas. This trends also found in the AHF estimations results, the industrial area has been decreased and the residential area has been increased. These things show that the COVID-19 affect to our life and urban environment in various ways.

From this study, we show the possibility to estimate the AHF from remotly sensed data and its accuracy by comparing with the actual energy consumption data. Because of the limitation of satellite images without clouds, we can only estimate two summer seasons of 2019 and 2020. In future works, if we can get more accurate images and detailed estimation method (equations), it can be used to monitor the AHF changes on urban areas.

Reference

1. Allen, R. G., Pereira, L. S., Raes, D., & Smith, M. (1998). Crop evapotranspiration-Guidelines for computing crop water requirements-FAO Irrigation and drainage paper 56. Fao, Rome, 300(9), D05109.
2. Allen, L., Lindberg, F., & Grimmond, C. S. B. (2011). Global to city scale urban anthropogenic heat flux: model and variability. International Journal of Climatology, 31(13), 1990-2005.
3. Bornstein, R. D. (1975). The two-dimensional URBMET urban boundary layer model. Journal of Applied Meteorology and Climatology, 14(8), 1459-1477.
4. Bornstein R, Lin Q. 2000. Urban heat islands and summertime convective thunderstorms in Atlanta: Three case studies. Atmospheric Environment. 34(3): 507-516.
5. Brutsaert, W. (1982). Evaporation into the atmosphere: Theory, history, and applications. D. Reidel Publ., Boston, MA. Evaporation into the atmosphere: Theory, history, and applications. D. Reidel Publ., Boston, MA.
6. Bueno, B., Pigeon, G., Norford, L. K., Zibouche, K., & Marchadier, C. (2012). Development and evaluation of a building energy model integrated in the TEB scheme. Geoscientific model development, 5(2), 433-448.
7. Chen, F., Yang, X., & Wu, J. (2016). Simulation of the urban climate in a Chinese megacity with spatially heterogeneous anthropogenic heat data. Journal of Geophysical Research: Atmospheres, 121(10), 5193-5212.
8. Conti, S., Meli, P., Minelli, G., Solimini, R., Toccaceli, V., Vichi, M., ... & Perini, L. (2005). Epidemiologic study of mortality during the Summer 2003 heat wave in Italy. Environmental research,

98(3), 390-399.
9. Cui, W., & Chui, T. F. M. (2021). Measurements and simulations of energy fluxes over a high-rise and compact urban area in Hong Kong. Science of The Total Environment, 765, 142718.
10. Doan, V. Q., Kusaka, H., & Nguyen, T. M. (2019). Roles of past, present, and future land use and anthropogenic heat release changes on urban heat island effects in Hanoi, Vietnam: Numerical experiments with a regional climate model. Sustainable Cities and Society, 47, 101479.
11. Flanner, M. G. (2009). Integrating anthropogenic heat flux with global climate models. Geophysical Research Letters, 36(2).
12. Gabey, A. M., Grimmond, C. S. B., & Capel-Timms, I. (2019). Anthropogenic heat flux: advisable spatial resolutions when input data are scarce. Theoretical and applied climatology, 135(1), 791-807.
13. Grimmond, C. S. B., Cleugh, H. A., & Oke, T. R. (1991a). An objective urban heat storage model and its comparison with other schemes. Atmospheric Environment. Part B. Urban Atmosphere, 25(3), 311-326.
14. Grimmond, C. S. B., & Oke, T. R. (1991b). An evapotranspiration interception model for urban areas. Water Resources Research, 27(7), 1739-1755.
15. Grimmond, C. S. B., & Oke, T. R. (2002). Turbulent heat fluxes in urban areas: Observations and a local-scale urban meteorological parameterization scheme (LUMPS). Journal of Applied Meteorology and Climatology, 41(7), 792-810.
16. Gutierrez, E., Gonzalez, J. E., Martilli, A., & Bornstein, R. (2015). On the anthropogenic heat fluxes using an air conditioning evaporative cooling parameterization for mesoscale urban canopy models. Journal of Solar Energy Engineering, 137(5), 051005.
17. Hamilton, I. G., Davies, M., Steadman, P., Stone, A., Ridley, I., &

Evans, S. (2009). The significance of the anthropogenic heat emissions of London's buildings: A comparison against captured shortwave solar radiation. Building and Environment, 44(4), 807-817.

18. Holtslag, A. A. M., & Van Ulden, A. P. (1983). A simple scheme for daytime estimates of the surface fluxes from routine weather data. Journal of Applied Meteorology and Climatology, 22(4), 517-529.
19. Iamarino, M., Beevers, S., & Grimmond, C. S. B. (2012). High& resolution (space, time) anthropogenic heat emissions: London 1970-2025. International Journal of Climatology, 32(11), 1754-1767.
20. Kato, S., & Yamaguchi, Y. (2005). Analysis of urban heat-island effect using ASTER and ETM+ Data: Separation of anthropogenic heat discharge and natural heat radiation from sensible heat flux. Remote Sensing of Environment, 99(1-2), 44-54.
21. Kato, S., & Yamaguchi, Y. (2007). Estimation of storage heat flux in an urban area using ASTER data. Remote Sensing of Environment, 110(1), 1-17.
22. Kikegawa, Y., Genchi, Y., Yoshikado, H., & Kondo, H. (2003). Development of a numerical simulation system toward comprehensive assessments of urban warming countermeasures including their impacts upon the urban buildings' energy-demands. Applied Energy, 76(4), 449-466.
23. Kwon, Y. J., & Lee, D. K. (2019). Thermal comfort and longwave radiation over time in urban residential complexes. Sustainability, 11(8), 2251.
24. Loridan, T., Grimmond, C. S. B., Offerle, B. D., Young, D. T., Smith, T. E., Jarvi, L., & Lindberg, F. (2011). Local-scale urban meteorological parameterization scheme (LUMPS): longwave radiation parameterization and seasonality-related developments. Journal of Applied Meteorology and Climatology, 50(1), 185-202.

25. Macdonald, R. W., Griffiths, R. F., & Hall, D. J. (1998). An improved method for the estimation of surface roughness of obstacle arrays. Atmospheric environment, 32(11), 1857-1864.
26. Oke, T. R. (1973). City size and the urban heat island. Atmospheric Environment (1967), 7(8), 769-779.
27. Oke, T. R. (1982). The energetic basis of the urban heat island. Quarterly Journal of the Royal Meteorological Society, 108(455), 1-24.
28. Oke, T. R., Spronken-Smith, R. A., Jauregui, E., & Grimmond, C. S. (1999). The energy balance of central Mexico City during the dry season. Atmospheric Environment, 33(24-25), 3919-3930.
29. Park, C. Y., Lee, D. K., Krayenhoff, E. S., Heo, H. K., Ahn, S., Asawa, T., ... & Kim, H. G. (2018). A multilayer mean radiant temperature model for pedestrians in a street canyon with trees. Building and Environment, 141, 298-309.
30. Radhi H, Fikry F, Sharples S. 2013. Impacts of urbanisation on the thermal behaviour of new built up environments: A scoping study of the urban heat island in Bahrain. Landscape and Urban Planning. 113: 47-61.
31. Sailor, D. J., & Lu, L. (2004). A top-down methodology for developing diurnal and seasonal anthropogenic heating profiles for urban areas. Atmospheric environment, 38(17), 2737-2748.
32. Smith, C., Lindley, S., & Levermore, G. (2009). Estimating spatial and temporal patterns of urban anthropogenic heat fluxes for UK cities: the case of Manchester. Theoretical and Applied Climatology, 98(1), 19-35.
33. Spronken Smith, R. A. (2002). Comparison of summer and winter time suburban energy fluxes in Christchurch, New Zealand. International Journal of Climatology: A Journal of the Royal Meteorological Society, 22(8), 979-992.
34. Yuan, C., Adelia, A. S., Mei, S., He, W., Li, X. X., & Norford, L.

(2020). Mitigating intensity of urban heat island by better understanding on urban morphology and anthropogenic heat dispersion. Building and Environment, 176, 106876.
35. Yu, C., Hu, D., Wang, S., Chen, S., & Wang, Y. (2021). Estimation of anthropogenic heat flux and its coupling analysis with urban building characteristics–A case study of typical cities in the Yangtze River Delta, China. Science of The Total Environment, 774, 145805.
36. Varquez, A. C. G., Kiyomoto, S., & Kanda, M. (2021). Global 1-km present and future hourly anthropogenic heat flux. Scientific data, 8(1), 1-14.
37. Zhang, X., Aono, Y., & Monji, N. (1998). Spatial variability of urban surface heat fluxes estimated from Landsat TM data under summer and winter conditions. Journal of Agricultural Meteorology, 54(1), 1-11.

Abstract

도시화가 진행됨에 따라 도시에서 발생하는 열의 양도 점차 증가하고 있다. 수송, 에너지 소비 등 인간 활동에 의해 발생하는 열을 뜻하는 인공열 플럭스(Anthropogenic Heat Flux)는 점차 증가하고 있으며, 도시의 열 환경을 이해는데 있어 중요한 요소로 주목받고 있다. 그러나 아직까지는 도시에서 발생하는 인공열 플럭스를 추정하는 정확한 방법이 존재하지 않아 어려움을 겪고 있다. 본 연구에서는 원격 탐사 데이터를 활용하여 대상지의 실제 열 환경을 최대한 반영할 수 있는 인공열 추정 방법을 제시하고자 한다. 인공열 플럭스 추정 결과 산업단지에서 가장 높은 평균값을 보였으며 이는 130 W/m^2로 가장 낮은 평균값을 보인 녹지의 10 W/m^2와 큰 차이를 보여주었다. 2019년과 2020년의 결과를 비교해보았을 때, 가산디지털단지와 관악구의 주거지역에서 큰 변화를 확인할 수 있었다. 가산디지털단지의 인공열 플럭스는 대상지 내에서 가장 크게 감소하였으며, 관악구의 주거지역은 가장 크게 증가하였다. 이 기간 동안 COVID-19의 영향으로 사회적 거리두기 정책이 시행되었으며, 그 영향으로 인해 시민들의 활동 양상에 큰 변화가 발생하게 되었다. 본 연구방법을 통한 추정 결과 역시 이러한 사회적 변화가 반영되어 위와 같은 결과를 나타낸 것으로 보인다. 에너지 소비량을 기반으로 추정한 인공열 플럭스와 본 연구방법을 통해 추정한 결과를 비교해보았을 때, 서로 간의 차이는 2019년, 2020년 각각 0.13, 0.22 W/m^2로 매우 작았으며 이를 통해 본 방법의 정확성을 간접적으로 확인할 수 있었다.

주요어 : 인공열, 도시 열섬, 위성 영상, 에너지 소비량, 도시 계획
학 번 : 2020-27283